Atmospheric Environment 44 (2010) 4081–4089

Contents lists available at ScienceDirect

Atmospheric Environment

journal homepage: www.elsevier.com/locate/atmosenv

Heterogeneous conversion of nitric acid to nitrous acid on the surface of primary organic aerosol in an urban atmosphere

Luke D. Ziemba [a,*], Jack E. Dibb [a], Robert J. Griffin [a,1], Casey H. Anderson [a], Sallie I. Whitlow [a], Barry L. Lefer [b], Bernhard Rappenglück [b], James Flynn [b]

[a] Institute for the Study of Earth, Oceans, and Space, Climate Change Research Center, University of New Hampshire, Durham, NH 03824, USA
[b] Department of Earth and Atmospheric Sciences, University of Houston, Houston, TX, USA

ARTICLE INFO

Article history:
Received 28 August 2008
Received in revised form
8 December 2008
Accepted 13 December 2008

Keywords:
HONO
HNO_3
Primary organic aerosol
AMS
Heterogeneous reaction

ABSTRACT

Nitrous acid (HONO), nitric acid (HNO_3), and organic aerosol were measured simultaneously atop an 18-story tower in Houston, TX during August and September of 2006. HONO and HNO_3 were measured using a mist chamber/ion chromatographic technique, and aerosol size and chemical composition were determined using an Aerodyne quadrupole aerosol mass spectrometer. Observations indicate the potential for a new HONO formation pathway: heterogeneous conversion of HNO_3 on the surface of primary organic aerosol (POA). Significant HONO production was observed, with an average of 0.97 ppbv event^{-1} and a maximum increase of 2.2 ppb in 4 h. Nine identified events showed clear HNO_3 depletion and well-correlated increases in both HONO concentration and POA-dominated aerosol surface area (SA). Linear regression analysis results in correlation coefficients (r^2) of 0.82 for HONO/SA and 0.92 for HONO/HNO_3. After correction for established HONO formation pathways, molar increases in excess HONO ($HONO_{excess}$) and decreases in HNO_3 were nearly balanced, with an average $HONO_{excess}/HNO_3$ value of 0.97. Deviations from this mole balance indicate that the residual HNO_3 formed aerosol-phase nitrate. Aerosol mass spectral analysis suggests that the composition of POA could influence HONO production. Several previously identified aerosol-phase PAH compounds were enriched during events, suggesting their potential importance for heterogeneous HONO formation.

1. Introduction

Nitrous acid (HONO) plays an important role in the cycling of both hydrogen (HO_x) and nitrogen (NO_x) oxides through the photolytic production of hydroxyl radical (OH) and nitrogen oxide (NO) (reaction (R1)) (Harrison et al., 1996; Alicke et al., 2003), especially during the early morning:

$$HONO + h\nu \xrightarrow{\lambda = 290–400\ nm} OH + NO \quad (R1)$$

The sources of HONO in urban atmospheres currently are not well understood. HONO formation was thought to occur heterogeneously by the hydrolysis of nitrogen dioxide (NO_2) (Finlayson-Pitts et al., 2003), a reaction that also produces nitric acid (HNO_3) (reaction (R2)):

$$2NO_2 + H_2O \xrightarrow{surface} HONO + HNO_3 \quad (R2)$$

The kinetic details regarding this reaction are not conclusive (Finlayson-Pitts et al., 2003 and references therein), but the reaction is likely first-order in NO_2.

Various environmentally relevant surfaces may contribute to HONO formation through reactions of NO_2. Soot aerosol has been identified as a likely reaction surface for HONO production by reaction (R3) (Ammann et al., 1998):

$$NO_2 + red_{ads} \rightarrow HONO + ox_{ads} \quad (R3)$$

where red_{ads} and ox_{ads} represent reduced and oxidized states, respectively, of the adsorbing soot surface. This reaction likely is favored compared to reaction (R2) because laboratory studies fail to detect HNO_3 as a major product (Ammann et al., 1998; Kalberer et al., 1999) and because of kinetic limitations of reaction (R2) compared to reaction (R3). Kalberer et al. (1999) reported reaction potentials (f_{soot}) for reaction (R3) that depend on relative humidity (RH), are insensitive to ozone (O_3) or NO_2 concentration, and are very fast. The maximum f_{soot} measured by Kalberer et al. (1999) was 1×10^{15} molec cm^{-2} at an RH of 30%. At an RH of 70%, Kalberer et al.

* Corresponding author. Tel.: +1 603 862 2382; fax: +1 603 862 2124.
E-mail address: lziemba@unh.edu (L.D. Ziemba).
[1] Present address: Department of Civil and Environmental Engineering, Rice University, Houston, TX, USA.

1352-2310/$ – see front matter © 2008 Elsevier Ltd. All rights reserved.
doi:10.1016/j.atmosenv.2008.12.024

(1999) report a decreased value for f_{soot} of approximately 0.2×10^{15} molec cm^{-2}. This is similar to the reaction potential of 0.25×10^{15} molec cm^{-2} reported later by Arens et al. (2001). The relevance of a net surface reaction such as reaction (R3) without a mechanism to recycle active surface sites is still unknown (Kalberer et al., 1999; Kleffmann et al., 1999). Such a mechanism has been proposed through additional soot-surface NO_2 reduction by water-soluble organic compounds such as phenols that better represent real automobile emissions (Gutzwiller et al., 2002; Ammann et al., 2005). Photo-dependent NO_2 reduction also has been observed on humic acid films (Stemmler et al., 2006) and films of aromatic organic compounds (George et al., 2005).

Nitric acid has been identified as a precursor to HONO in various atmospheres (Clemitshaw, 2006). Laboratory work suggests the potential for HNO_3 surface photolysis resulting in HONO and NO_2 production by reaction (R4) (Zhou et al., 2003):

$$\begin{aligned} &HNO_{3(ads)} \xrightarrow{h\nu} [HNO_3]^*_{(ads)} \\ &[HNO_3]^*_{(ads)} \rightarrow HNO_{2(ads)} + O(^3P)_{(ads)} \\ &[HNO_3]^*_{(ads)} \rightarrow NO_{2(ads)} + OH_{(ads)} \end{aligned} \quad \text{(R4)}$$

where O (^{3}P) is the oxygen atom. Photolysis of HNO_3 on surfaces occurs at a much faster rate than in the gas phase or in bulk solution. Using an HNO_3-coated flow reactor, Zhou et al. (2003) derived a photolysis rate constant (j_{HNO_3-HONO}) for HONO production of 1.2×10^{-5} s^{-1} at 50% RH. At 80% RH, j_{HNO_3-HONO} increased to 1.4×10^{-5} s^{-1} due to intermediate production of NO_2 and subsequent conversion to HONO. Modeling has suggested that an HNO_3 photolysis mechanism was important for HONO production during the 2001 Northeast Oxidant and Particle Study (Sarwar et al., 2008). Inclusion of renoxification processes on surfaces enhanced HONO concentrations significantly (by an order of magnitude), and improved O_3 model performance, in the South Coast Air Basin of California (Knipping and Dabdub, 2002).

Another mechanism of HONO formation involves the reaction of HNO_3 with NO (Rivera-Figueroa et al., 2003) on hydrated glass surfaces by reaction (R5) via a photochemically independent heterogeneous pathway:

$$HNO_3 + NO \xrightarrow{\text{surface}} HONO + NO_2 \quad \text{(R5)}$$

Additionally, laboratory work has shown that dissolved nitrate ion (NO_3^-), not simply adsorbed HNO_3, contributes to HONO and NO_2 formation on organic films (Handley et al., 2007). While HONO formation has been observed in laboratory experiments and mechanisms for these processes have been suggested, modeling studies consistently underestimate ambient HONO concentrations (Moussiopoulos et al., 2000; Vogel et al., 2003) despite emphasizing the importance of heterogeneous processing.

This work indicates significant HONO production in the Houston, TX atmosphere correlated strongly with depletion of HNO_3 and enhanced hydrocarbon-like organic aerosol (HOA) surface area. Such events, which typically occurred during early morning, indicate a potential new HONO formation pathway: heterogeneous conversion of HNO_3 to HONO on primary HOA. Because of the many co-dependent variables in question, the mechanism of HONO formation cannot be determined explicitly. However, it is clear that the magnitude of the observed HONO cannot be explained without a currently unidentified source.

2. Methods

2.1. Measurements

All gas- and aerosol-phase measurements were made between 20 August 2006 and 27 September 2006 during the Texas Air Quality Study II Radical and Aerosol Measurement Project (TRAMP, Lefer and Rappengluck, this issue). Sampling instrumentation was located atop the North Moody Tower, an 18-story building on the campus of the University of Houston. Nitric and nitrous acid observations were made by a mist chamber/ion chromatographic (MC/IC) technique (Scheuer et al., 2003; Dibb et al., 2004). Air was sampled through a heated inlet designed specifically to eliminate loss of HNO_3 during sampling. Acidic gases (HNO_3, HONO, and hydrochloric acid) were removed over 5-min periods from the air by the MC, collected into 13–15 ml (depending on ambient RH) of pure water, and immediately and automatically quantified by IC. Two identical MC/IC systems were used alternately to obtain continuous measurements. Direct comparison between this measurement and HONO measured by long-path differential optical absorption spectroscopy yielded excellent agreement (Stutz et al., this issue), especially during the early morning period of focus in this study.

Aerosol mass concentrations and mass size distributions of non-refractory aerosol between 40 and 1000 nm in vacuum aerodynamic diameter (D_{VA}) were measured by an Aerodyne quadrupole aerosol mass spectrometer (Q-AMS). Specific information regarding instrument design, quantification, and field deployment has been well documented previously (Jayne et al., 2000; Jimenez et al., 2003; Canagaratna et al., 2007). The quantification of particle-phase nitrate is based on the sum of mass spectral signal at mass-to-charge ratio (m/z) = 30 and m/z = 46 (the fragments NO^+ and NO_2^+, respectively) measured by the Q-AMS. This quantification is complicated by potential contribution of organic compounds (Bae et al., 2007), or other nitrogen-containing compounds such as amines, to signal at m/z = 30. Therefore, particle-phase nitrate could be overestimated here, as the average ambient m/z 30 to 46 ratio was 5.0 compared to a value of 2.15 for pure ammonium nitrate (NH_4NO_3) measured during calibrations. However, the contribution of organic fragments to m/z = 30 signal was less significant during the HONO events discussed in Section 4.1 (compared to measurements made during the afternoon): the measured m/z 30 to 46 ratio was 4.2 during these periods.

The mass spectral signal at m/z = 44 has been used as a tracer for oxidized organic aerosol (OOA), and the signal at m/z = 57 has been used as a tracer for HOA (Zhang et al., 2005a). Additionally, organic mass spectra were compared by normalizing each m/z signal to the total mass loading for that time period. These values are denoted by X, where, for example, X_{44} is the fraction of the total organic mass spectral signal that was observed at m/z = 44. These comparisons are discussed further in Sections 3.3 and 4.3.

Additional supporting data were collected as follows (Lefer et al., this issue): NO and NO_x were measured using a modified trace-level Thermo Environmental (TEI) 42c NO + O_3 chemiluminescence instrument. The instrument was modified with an externally mounted light-emitting diode-based blue light converter that selectively dissociates NO_2 to NO. Carbon monoxide (CO) was measured using a TEI 48c trace-level enhanced gas filter correlation wheel instrument. Acetylene was measured together with a large suite of other volatile organic compounds (VOCs) online every hour using a Perkin–Elmer VOC-system (Leuchner and Rappengluck, this issue). Supplemental meteorological data were also available (Lefer et al., this issue).

2.2. Total aerosol surface area

Aerosol mass size distributions measured by the Q-AMS in particle time-of-flight mode were used to calculate total aerosol surface area (SA) for each 10-min sampling period. Calculations were based on summed Q-AMS aerosol mass

(sulfate + nitrate + ammonium + organics + chloride) assuming spherical particles of a uniform density of 1.2 g cm^{-3}. SA was calculated by

$$SA = \sum_{D_{VA}=40\ nm}^{D_{VA}=1000\ nm} \left[\frac{\text{Aerosol Mass}_{AMS(D_{VA})}}{\text{Aerosol density}} \frac{6}{D_{VA}}\right] \quad \left(\mu m^2\ cm^{-3}\right) \tag{1}$$

2.3. Rush hour definition

To focus on the morning hours during which events (described in more detail subsequently) generally occurred, the full dataset was segregated into two subsets. Data collected between 0500 and 0850 CST are henceforth termed 'morning rush hour' (MRH) data while data from the remainder (0900–0450 CST) will be referred to as 'non-morning rush hour' (non-MRH) data. Selection of the MRH interval was based solely on the diurnal profile of CO, a tracer of urban combustion. Carbon monoxide peaked at a median concentration of 308 ± 185 ppb (90th percentile of 682 ppb) at 0700 CST. During non-MRH periods, the median CO concentration was 186 ± 85 ppb. The average acetylene mixing ratio during MRH was 924 ppt, compared to a full-campaign median value of 586 ppt, indicating that combustion sources are likely important during this time (Harley et al., 1992). Because of timing and association with increased CO and acetylene, MRH air masses likely are dominated by local automobile exhaust although possible influence of the nearby Houston Ship Channel (HSC) on MRH chemistry cannot be excluded.

3. Results

3.1. Interaction between HONO, particle-phase nitrate, and HNO_3

The diurnal patterns of HONO, particle-phase nitrate, and HNO_3 exhibited very different characteristics. Fig. 1 shows a diurnal box plot of these three species over the full campaign. Both HONO and particle-phase nitrate had clear peaks in median, 75th percentile, and 95th percentile concentrations between 0600 and 0800 CST, with a HONO median concentration of 23.2 nmol m^{-3} and a median particle-phase nitrate concentration of 0.590 μg m^{-3}. Contrarily, minimum median concentrations of HNO_3 were observed during these hours (22.3 nmol m^{-3}), and a clear daytime median peak of 84.9 nmol m^{-3} was observed at 1200 CST.

The daytime maximum in HNO_3 is consistent with dominant photochemical production by the reaction between NO_2 and OH. Decreased daytime concentrations of HONO likely are explained by the dominance of photolytic loss (reaction (R1)) over production by all mechanisms including the reverse of reaction (R1). An anti-correlation between HONO and HNO_3 for the full measurement campaign is clearly shown in Fig. 1. Time-series data (not shown) indicated that morning decreases in HNO_3 were more often than not accompanied by increases in HONO. Small daytime concentrations of particle-phase nitrate are likely due to both the relatively high vapor pressure of NH_4NO_3 and a lack of available ammonia. Non-MRH aerosols were not fully neutralized, with an average sulfate to ammonium molar ratio of 1.36, making NH_4NO_3 formation thermodynamically unfavorable.

3.2. Surface area dependence

Significant increases in calculated SA were observed during MRH and were driven by variability in organic aerosol. Calculated median aerosol surface area was increased by 24% during MRH (287 μm^2 cm^{-3}) compared to the SA for non-MRH periods (232 μm^2 cm^{-3}). The difference between 90th percentile SA for MRH and non-MRH periods,

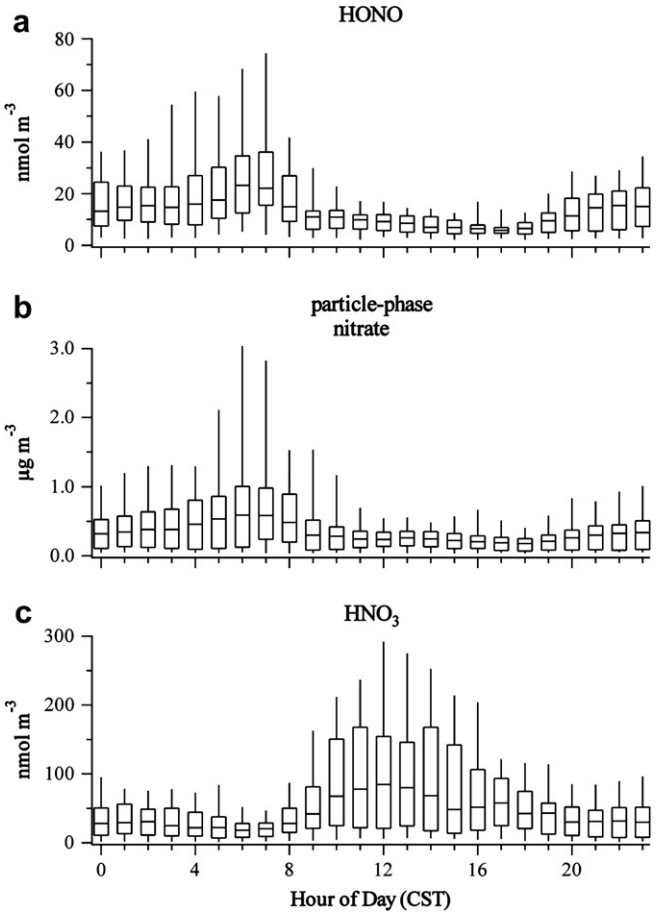

Fig. 1. Full-campaign diurnal plots for a.) HONO, b.) particle-phase nitrate, and c.) HNO_3. The line inside of each box represents the median concentration, the top and bottom of each box represent the 75th and 25th percentile concentrations, respectively, and the top and bottom of each whisker represent the 95th and 5th percentile concentrations, respectively.

an increase of over 40%, is even larger. The peak in SA occurs at 0700 CST, similar to the diurnal profile of HONO and particle-phase nitrate. A linear regression (Fig. 2) shows a strong correlation between organic aerosol and SA during MRH, with a correlation coefficient (r^2) of 0.95, indicating that almost all of the variability in SA during MRH can be explained by changes in organic aerosol. By contrast, sulfate aerosol (not shown in Fig. 2 but included in Figs. 3 and 4) was not well correlated with SA ($r^2 = 0.54$), especially at high SA. MRH HONO concentrations were also well correlated with SA, with a correlation coefficient of 0.82 and a slope (the HONO reaction potential with respect to SA) of 5.0×10^{15} molec cm^{-2} (Fig. 2).

3.3. Aerosols during MRH

Significant chemical differences were observed between MRH and non-MRH aerosol. The median aerosol mass concentration during MRH periods (11.8 μg m^{-3}) was 25% larger than the mass concentration during non-MRH periods (9.45 μg m^{-3}). Aerosol mass during MRH was dominated by organics, which constituted 59% of the total aerosol mass, compared to a composition of 51% organic mass during non-MRH sampling. This difference is driven by an average MRH increase of 2.0 μg m^{-3} in organic concentration with no corresponding change in sulfate or ammonium concentration (−0.03 and 0.02 μg m^{-3}, respectively). The constant sulfate concentrations during MRH (clearly evident during the events in Figs. 3 and 4) are consistent with a traffic fleet dominated by

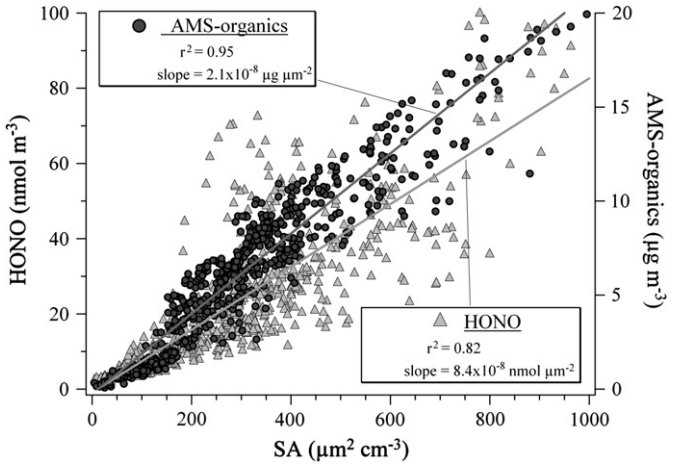

Fig. 2. Linear regression of HONO and organic aerosol versus SA for only MRH data. Slopes include appropriate unit conversions.

gasoline fueled cars and light-duty trucks (McGaughey et al., 2004) that do not emit significant quantities of sulfur dioxide. Median particle-phase nitrate concentrations increased by 120% during MRH periods compared to the non-MRH periods, which is also seen in the diurnal analysis in Fig. 1.

Significant differences between MRH and non-MRH aerosols were observed in the Q-AMS mass spectra. The median ratio of $m/z = 44/57$, was largest during times when photochemistry dominated (9.1 for the 1500 CST hour) and was smallest during MRH (2.6 for the 0700 CST hour), an indication that MRH organic aerosol is less oxidized and more like HOA. Elevated CO and acetylene concentrations coincident with decreased $m/z = 44/57$ strongly indicate that HOA is primary in nature.

Mass spectra measured by the Q-AMS for MRH organic aerosol were compared to non-MRH organic aerosol using the ratio of X_{MRH}/X_{nMRH} shown in Fig. 5a ($m/z < 200$) and Fig. 6a ($m/z > 200$). MRH organic aerosol was enriched at larger m/z fragments, exclusively after $m/z = 114$, and depleted in smaller m/z. MRH aerosol was enriched by more than 38% at $m/z = 57$ (highlighted in Fig. 5), which likely represents the $C_4H_9^+$ fragment (Zhang et al., 2005b). Other notably enriched m/z signals were observed at larger m/z in intervals of approximately 12 and 14 m/z units, at $m/z = 69$, 71, 81, 83, 93, and 95. These signals likely are due to the addition of C^+ and CH_2^+ fragments to $C_4H_9^+$ fragments. All of the MRH-enriched m/z signals mentioned above have been observed prominently in diesel exhaust (Canagaratna et al., 2004) and ambient urban aerosol (Alfarra et al., 2004; Zhang et al., 2005b). Contrary to observations during the previously mentioned studies of diesel and urban aerosol, $m/z = 43$ was enriched by less than 5% during MRH. This is likely due to the prominence of $m/z = 43$ in oxidized organic aerosol during the daytime as well as during MRH. Signal at $m/z = 44$ (highlighted in Fig. 5), the fingerprint often used to identify oxidized (and likely processed) organic aerosol, was depleted during MRH by approximately 14%. Laboratory work involving diesel exhaust processing has shown that $m/z = 44$ becomes increasingly important with photochemical age (Sage et al., 2008), suggesting that MRH aerosol is less processed and relatively fresh photochemically. Signal at $m/z = 60$ (potentially $C_2H_4O_2^+$) and signals at m/z associated with subsequent additions of CH_n^+ fragments (at $m/z = 73$, 87, 100, and 114) were also observed to be depleted during MRH. These fragments were similarly not observed in diesel and urban aerosols (Zhang et al., 2005a). Thus, the mass spectral signature observed during MRH and documented in Fig. 5 is consistent with HOA that was emitted.

4. Discussion

4.1. Observation of heterogeneous HONO formation events

Concentrations of HONO in the Houston urban atmosphere were enhanced significantly during MRH periods. This time period was dominated by vehicular emissions that significantly increased aerosol SA, nearly entirely due to increased abundance of primary HOA. This correlation indicates the potential importance of heterogeneous processes driving HONO formation. The good correlation between HONO and SA suggests that aerosol surface is the dominant reaction substrate and that stationary sources (buildings, soils, etc.) are likely unimportant, a supposition supported by modeling (Stutz et al., this issue). Boundary layer

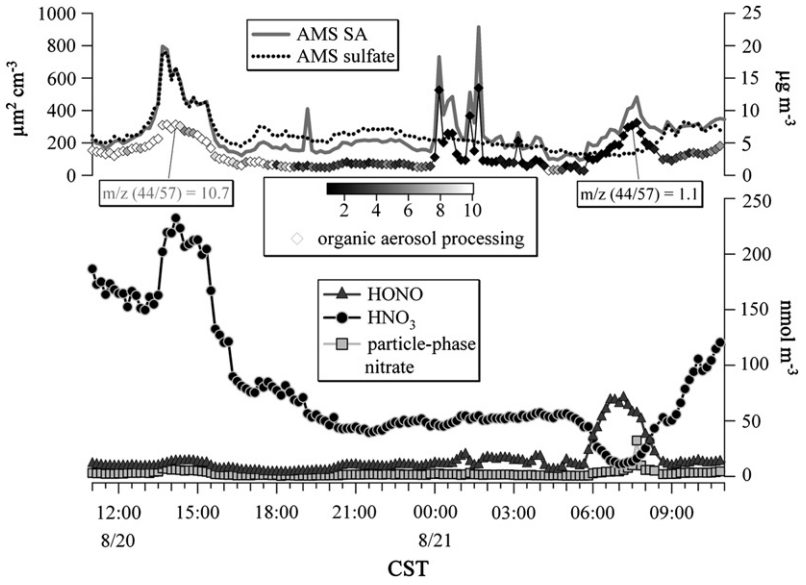

Fig. 3. 21 August event. Organic processing is described by $m/z = 44/57$, as described in the text.

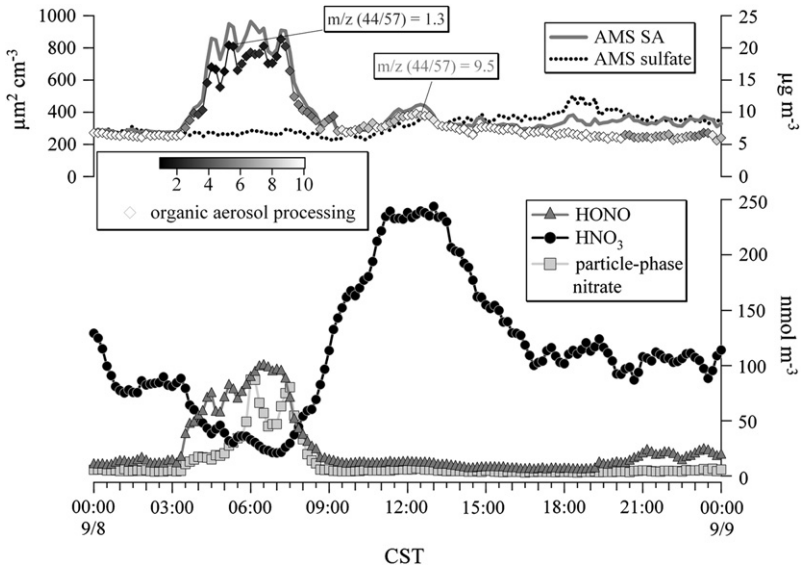

Fig. 4. 8 September event. Organic processing is described by $m/z = 44/57$, as described in the text.

dynamics can be ruled out as a complicating factor because other atmospheric components with negligible MRH sources, such as sulfate aerosol, showed no correlated increase (Figs. 3 and 4).

Enhanced HONO concentrations during MRH frequently were accompanied by significant depletion in HNO_3. To explore the possibility that HNO_3 is a potential precursor to HONO, events were identified that were characterized by both an increase in HONO concentration and a decrease in HNO_3 concentration. Two examples of such events are presented in Figs. 3 and 4. Start and end times for all events (Table 1) were defined based on visual inspection of HNO_3 data such that the events on 21 August and 8 September (Figs. 3 and 4) start at 0540 and 0320 CST, respectively. These events show clearly the anti-correlation between HONO and HNO_3, as well as the coincident enhancement of less-processed organic aerosol and SA during MRH. The contrast between HOA-dominant and OOA-dominant organic aerosol between MRH and mid-afternoon is emphasized.

Linear regression analysis was performed for each event to assess the dependence of HONO on SA and of HONO on HNO_3. To isolate potential heterogeneous processing, only data from the onset of HNO_3 depletion to the maximum observed HONO concentration were used for linear regression analysis, as measurements after the HONO peak likely are complicated by increasing photolytic HONO loss (by reaction (R1)) and photochemical HNO_3 production (from OH and NO_2). Nine events were observed throughout the campaign, and slopes and correlation coefficients for each of these events are reported in Table 1. The change in HONO during each event (ΔHONO) is also included in Table 2 and was calculated as the difference between the peak HONO concentration and the concentration at the start of the event. Each event exhibited significant ΔHONO, especially the 21 August and 8 September events (shown in Figs. 3 and 4) during

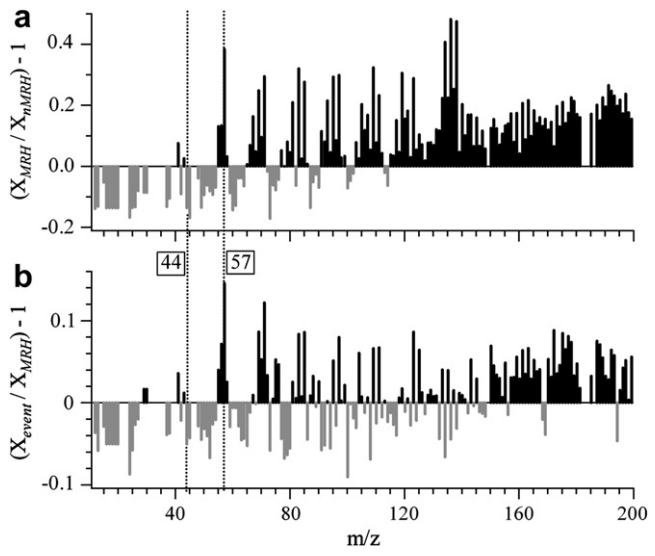

Fig. 5. Comparison of organic aerosol mass spectra (up to $m/z = 200$) for a.) MRH (X_{MRH}) and non-MRH (X_{nMRH}) and b.) the event-average mass spectra (X_{event}) and X_{MRH}. Values above zero (in black) indicate m/z signals that were enriched. Values below zero (in gray) indicate m/z signals that were depleted. Signals at $m/z = 44$ and 57 are highlighted. Note that the scale is reduced for b.).

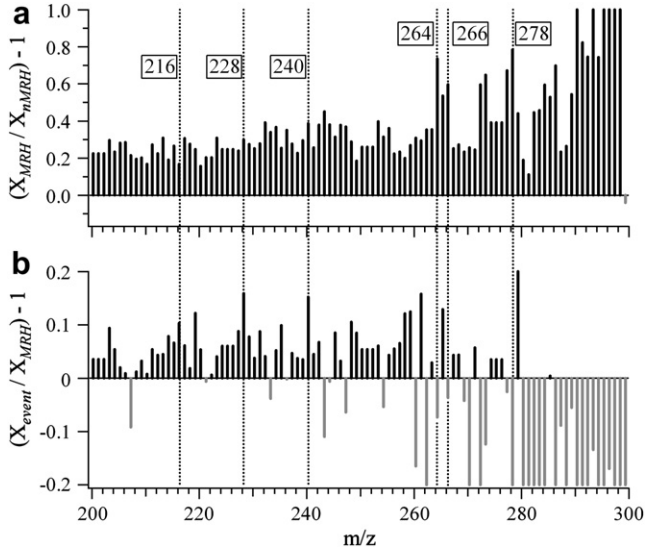

Fig. 6. Comparison of organic aerosol mass spectra (m/z from 200 to 300) for a.) MRH (X_{MRH}) and non-MRH (X_{nMRH}) and b.) the event-average mass spectra (X_{event}) and X_{MRH}. Values above zero (in black) indicate m/z signals that were enriched. Values below zero (in gray) indicate m/z signals that were depleted. Signals at $m/z = 216$, 228, 240, 264, 266, and 278 are highlighted. Note that the scale is reduced for b.).

Table 1
Linear regression analysis for HNO_3 depletion events. Slopes presented here include relevant unit conversions.

	Linear regression: HONO/SA ($\times 10^{15}$ mol cm^{-2})	Linear regression: HONO/HNO_3 (nmol/nmol)	Linear regression: $HONO_{excess}$/HNO_3 (nmol/nmol)[a]
21-Aug (0540–0840),[b] SR[c] = 0552	Slope = 18(5.5),[d] $r^2 = 0.92$	Slope = −1.6(0.22), $r^2 = 0.98$	Slope = −1.0(0.18), $r^2 = 0.97$
22-Aug (0630–0830), SR = 0553	Slope = 9.6(1.4), $r^2 = 0.99$	Slope = −3.6(0.66), $r^2 = 0.98$	Slope = −1.9(0.64), $r^2 = 0.96$
31-Aug (0230–0510), SR = 0558	Slope = 4.1(2.2), $r^2 = 0.80$	Slope = −1.1(0.45), $r^2 = 0.87$	Slope = −0.70(0.66), $r^2 = 0.73$
2-Sep (0110–0240), SR = 0559	Slope = 7.2(2.3), $r^2 = 0.88$	Slope = −0.55(0.28), $r^2 = 0.77$	NA[e]
2-Sep (0450–0820), SR = 0559	Slope = 3.4(1.4), $r^2 = 0.81$	Slope = −0.65(0.12), $r^2 = 0.95$	Slope = −0.37(0.33), $r^2 = 0.60$
4-Sep (0350–0710), SR = 0600	Slope = 2.3(2.1), $r^2 = 0.57$	Slope = −0.75(0.18), $r^2 = 0.94$	Slope = −0.79(0.44), $r^2 = 0.76$
7-Sep (0350–0730), SR = 0602	Slope = 5.0(0.90), $r^2 = 0.95$	Slope = −1.1(0.26), $r^2 = 0.92$	Slope = −0.40(0.34), $r^2 = 0.61$
8-Sep (0320–0820), SR = 0602	Slope = 4.9(1.2), $r^2 = 0.89$	Slope = −1.2(0.19), $r^2 = 0.95$	Slope = −1.0 (0.23), $r^2 = 0.91$
15-Sep (0700–0900), SR = 0606	Slope = 2.9(1.6), $r^2 = 0.86$	Slope = −2.6(0.67), $r^2 = 0.96$	Slope = −1.6 (0.30), $r^2 = 0.98$

[a] Corresponding to the likely scenario described in Section 4.2.
[b] Start and stop time of event in CST.
[c] Time of sunrise (SR) in CST.
[d] Twice standard deviation of computed slope in parentheses.
[e] Sufficient data not available to calculate $HONO_{excess}$.

which ΔHONO was 1.48 and 2.18 ppb (60.5 and 89.2 nmol m^{-3}), respectively.

Excellent correlation was found for both HONO/SA and HONO/HNO_3 during all events (Table 1). The average HONO/SA slope for the nine events was $6.6 \pm 2.0 \times 10^{15}$ molec cm^{-2}, slightly larger than the MRH slope shown in Fig. 2. The absolute value of the slope of a regression between HONO and HNO_3 can be interpreted as a mole balance between precursor and product. Here, it is assumed that 1 mol of HNO_3 produces 1 mol of HONO and that no other species contribute to HONO formation. This assumption is likely incorrect, so the HONO/HNO_3 slopes are not expected to be unity (Table 1). The average HONO/HNO_3 slope for all nine observed events was 1.5 ± 0.34, indicating that the moles of depleted HNO_3 (on average) cannot account for every mole of HONO formed. This suggests the likelihood of additional pathways contributing to HONO formation that do not involve HNO_3. A HONO–HNO_3 slope smaller than unity, during events on 2 September and 4 September, for example, indicates that the molar magnitude of HNO_3 depletion is larger than that of HONO formed. Thus, additional coincident HNO_3 loss pathways must exist. The observation of coincident increases in particle-phase nitrate during events could explain a portion of this excess HNO_3 and will be discussed further below. The observed HONO–HNO_3 slopes likely result from a combination of both scenarios.

4.2. Estimation of $HONO_{theoretical}$ and an $HONO_{excess}/HNO_3$ mole balance

To assess the potential contribution of HNO_3 to HONO formation, production from established mechanisms was considered quantitatively first. A theoretical HONO concentration ($HONO_{theoretical}$) was determined based on the known formation mechanisms outlined in Section 1 using measured NO_x (NO_{xobs}), NO_2 (NO_{2obs}), and SA (SA_{obs}) concentrations. Along with direct emissions, three heterogeneous reactions were considered as HONO sources: NO_2 hydrolysis by reaction (R2), NO_2 redox reactions on soot aerosol by reaction (R3), and HNO_3 surface photolysis by reaction (R4). Homogeneous reaction mechanisms were neglected based on modeling results (Moussiopoulos et al., 2000; Vogel et al., 2003; Sarwar et al., 2008) that suggest gas-phase reactions contribute negligibly to HONO formation compared to heterogeneous reactions and direct emissions. HONO production by reaction (R5) was also neglected because reaction kinetics are likely too slow (Rivera-Figueroa et al., 2003). Also, gas- and aqueous-phase HNO_3 photolysis is neglected due to rates approximately two orders of magnitude smaller than the surface photolysis rate reported by Zhou et al. (2003). The calculation of $HONO_{theoretical}$ is given by:

$$\begin{aligned} HONO_{theoretical} = {} & [f_{soot} \times SA_{obs}] + [NO_{Xobs} \times f_{emiss}] \\ & + [\Delta HNO_{3obs} \times \{1 - \exp(-j_{HNO_3-HONO} \times t)\}] \\ & + [NO_{2obs} \times \{1 - \exp(-k_2 \times t)\}] \end{aligned} \quad (2)$$

where f_{emiss} is the emission ratio of HONO to NO_x (ppb/ppb), ΔHNO_{3obs} is the change in observed HNO_3 concentration compared to the previous data point, k_2 is the reaction rate coefficient for reaction (R2), and t is the sampling duration for each data point (10 min).

The excess HONO concentration ($HONO_{excess}$), or the concentration formed in excess of that generated by established mechanisms, was calculated as the difference between the observed ($HONO_{obs}$) and $HONO_{theoretical}$ concentrations by equation (3):

$$HONO_{excess} = HONO_{obs} - HONO_{theoretical} \quad (3)$$

$HONO_{theoretical}$ and $HONO_{excess}$ were calculated for each data point used previously for determination of HONO/SA and HONO/HNO_3 in Table 1. It should be noted that the above calculation is meant to serve as a comparison to HNO_3 depletion, not a quantitative HONO formation model.

Two scenarios regarding $HONO_{theoretical}$ were computed according to the values listed in Table 3. The likely scenario is meant to be most applicable to conditions during observed Houston MRH events (high NO_2, high RH, and suitable aerosol surface area, reported in Table 2). The upper-limit scenario considers parameters that would result in maximum HONO production but were derived from less realistic conditions. The upper-limit f_{emiss} value used here is taken from the study of Kurtenbach et al. (2001) that was based on a traffic distribution

Table 2
Supporting measurements during HNO_3 depletion events.

	$m/z = 44/57$	Particle-phase nitrate (μg m^{-3})	Ave. RH (%)	Ave. NO_2, Peak NO_x (ppb)	ΔHONO (ppb)
21-Aug	1.1	0.39	78	29, 161	1.5
22-Aug	1.2	0.28	76	26, 149	1.0
31-Aug	2.5	0.95	65	49, 139	0.60
2-Sep	7.6	0.94	76	NA[c]	0.43
2-Sep	3.6	1.9	76	39, 96	0.98
4-Sep	5.3	0.83	74	21, 36	0.17
7-Sep	3.8	1.7	78	46, 91	0.87
8-Sep	3.6	2.2	74	50, 174	2.2
15-Sep	1.8	0.61	80	31, 107	0.44
Event Average	3.5	1.3	75	38,119	0.91
Full campaign[a]	5.8	0.38	65	20,77	–
MRH[b]	3.6	0.73	75	27,77	–

[a] 20 August through 27 September.
[b] 0500–0850 of full campaign.
[c] NA: not available.

Table 3
Values used for calculated $HONO_{theoretical}$ scenarios.

Parameter	Mechanism	Likely	Upper limit
f_{soot} (mol cm^{-2})	NO_2 reduction on soot aerosol[a]	0.2×10^{15}	1.0×10^{15}
f_{emiss} (ppb/ppb)	HONO emission factors[b,c]	0.003	0.008
j_{HNO_3-HONO} (s^{-1})	HONO from surface HNO_3 photolysis[d]	0.2×10^{-5}	1.4×10^{-5}
k_2 (min^{-1} m^{-1})[e]	NO_2 hydrolysis[c]	$0.003 \times (S/V)$	$0.003 \times (S/V)$

[a] Kalberer et al. (1999).
[b] Kirchstetter et al. (1996).
[c] Kurtenbach et al. (2001).
[d] Results from (Zhou et al., 2003) at 1200 CST (upper limit) and 0700 CST (likely).
[e] (S/V) = aerosol surface to volume ratio.

weighted more heavily by diesel and heavy-duty vehicles. The likely f_{emiss} is taken from Kirchstetter et al. (1996) and is based on tunnel studies of mostly light-duty, gasoline motor vehicles (similar to the assumed distribution during Houston MRH). Values for f_{soot} are from Kalberer et al. (1999) and are based on 70% RH for the likely scenario and on 30% RH for the upper-limit scenario. Only reaction potential, and not kinetic limitations, was considered for reaction (R3). Values for j_{HNO_3-HONO} are from Zhou et al. (2003) and are based on photolysis at 0700 CST for the likely scenario and on photolysis at 1200 CST for the upper-limit scenario. The value for k_2 is based on the results from Kurtenbach et al. (2001).

For the likely scenario, the average $HONO_{theoretical}$ was 23% of average $HONO_{obs}$, with a contribution range of 4.1–43%. Even when assessing the upper-limit $HONO_{theoretical}$ concentration, which is unrealistic for the conditions during events, the average contribution of $HONO_{theoretical}$ to $HONO_{obs}$ was just 78%. This is shown in Fig. 7, and indicates that the majority of the observed HONO could not be attributed to the major sources considered. Thus, an additional source must exist. For the likely scenario, direct emissions accounted for 90% of $HONO_{theoretical}$, and soot redox reaction accounted for 10%. Surface HNO_3 photolysis and NO_2 hydrolysis were negligible. The distribution is shifted slightly for the upper-limit scenario, with 71% of $HONO_{theoretical}$ due to emissions and 29% due to soot redox reactions.

Linear regressions for $HONO_{excess}$ (using the likely scenario) and HNO_3 for each event are described in Table 1. Excellent correlation coefficients were obtained for all events, with all $r^2 > 0.60$. The event-average $HONO_{excess}/HNO_3$ slope of 0.97 indicates that, overall, the depleted HNO_3 is nearly balanced by the HONO gained during MRH events, suggesting that HNO_3 is the missing source discussed above. Four of the eight applicable event slopes are statistically (within 2 standard deviations) unity while two event slopes are greater than unity and two are smaller. Both events with $HONO_{excess}/HNO_3$ less than unity (2 September and 7 September) exhibited weaker correlations (0.60 and 0.61, respectively), suggesting a potential missing HNO_3 sink during these events. In fact, these events were marked by notably enhanced particle-phase nitrate concentrations (Table 2; 1.9 and 1.7 μg m^{-3}, respectively), suggesting that much of the depleted HNO_3 that did not form HONO could have remained in the aerosol phase. Excluding the event on 8 September which exhibited very high particle-phase nitrate, the $HONO_{excess}/HNO_3$ mole balance was anti-correlated ($r^2 = 0.78$) with particle-phase nitrate, supporting the idea that particle-phase nitrate contributed to the $HONO_{excess}/HNO_3$ mole balance discrepancy. Inclusion of the outlying point for 8 September results in a weaker, but still significant, anti-correlation ($r^2 = 0.65$). The quantitative contribution of particle-phase nitrate to depleted HNO_3 is unknown, as speciation of the $m/z = 30$ signal from the Q-AMS is uncertain. Still, this anti-correlation seems to indicate strongly that particle-phase nitrate plays a role in HONO formation during MRH events.

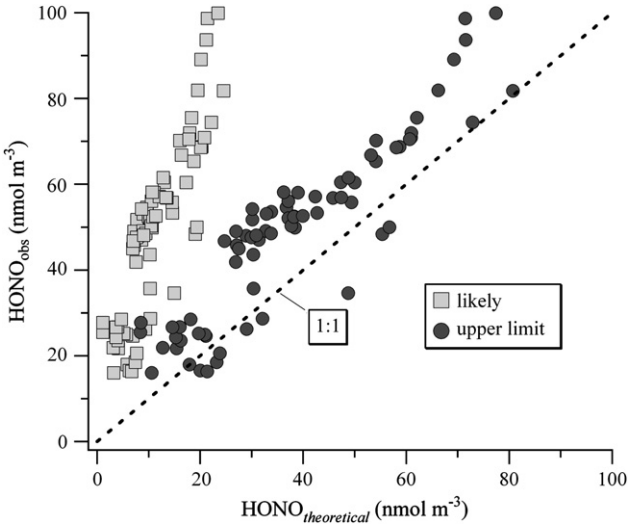

Fig. 7. Observed HONO concentrations versus theoretical HONO concentrations calculated using equation (2). The likely and upper-limit calculations are described in Section 4.2 and Table 3. Note that $HONO_{theoretical}$ does not include a potential heterogeneous HNO_3 source.

The two events with $HONO_{excess}/HNO_3$ slopes greater than unity (22 August and 15 September) likely are due to underestimation of HONO formed from NO_2 reactions. Both events were characterized by very high NO_x concentrations. One distinguishing characteristic of these events is decreased $m/z = 44/57$ signal (from Table 2; 1.2 and 1.8, respectively) from the Q-AMS, indicating that aerosol during these events was even less oxidized than in other MRH events. This could have resulted in more efficient reduction of NO_2 to HONO by reaction (R3) and an underestimation of $HONO_{theoretical}$, resulting in the calculated $HONO_{excess}/HNO_3$ slope that is greater than unity.

While no mechanistic information regarding the formation of $HONO_{excess}$ can be derived from the current observations, the process likely is not photo-dependent. This hypothesis is based on the observation of HONO formation prior to sunrise (Table 1) during several events (31 August, 2 September, 4 September, and 7 September). The lack of photo-dependence is most notable on 8 September (Fig. 4) when the HONO increase and HNO_3 depletion started well before the 0603 CST sunrise.

4.3. Organic aerosol composition during HONO events

Some evidence for a dependence of $HONO_{excess}$ production on organic aerosol composition exists. Mass spectral signals typical of HOA ($m/z = 57$, 71, etc.) discussed previously are enhanced in MRH compared to non-MRH as well as during events compared to MRH. Additionally, some correlation exists between X_{event}/X_{MRH} (for individual events) with ΔHONO and with computed HONO/SA slopes. For example, 21 August exhibited the largest $X_{57,event}/X_{57,MRH}$ for any event (an increase of 92%), a ΔHONO of 1.5 ppbv (61 nmol m^{-3}, Table 2), and the largest HONO/SA observed (Table 1). Likewise, the $X_{57,event}/X_{57,MRH}$ for 4 September was −0.34 (a decrease in $m/z = 57$ signal compared to the average $m/z = 57$ signal during MRH), corresponding to a minor ΔHONO of 0.17 ppbv (7.0 nmol m^{-3}, Table 2) and HONO/SA slope of 2.3 (Table 1). A chemical composition dominated by $m/z = 57$ likely represents a more reduced aerosol surface (compared to a composition dominated by $m/z = 44$). Thus, these results suggest a dependence of HONO production on the composition of HOA and potentially on the oxidation state of the HOA surface.

A recent study in Mexico City, another highly polluted urban center, identified several polycyclic aromatic hydrocarbons (PAHs) in the aerosol phase using a Q-AMS (Dzepina et al., 2007). To explore the potential influence of PAH during MRH and HONO events, X_{MRH}/X_{nMRH} and X_{event}/X_{MRH} spectra were compared to the PAH spectra obtained by Dzepina et al. (2007). Since most of the PAH signal is observed at $m/z > 200$, this mass spectral region is the focus of Fig. 6. Out of the eight molecular ion signals (or groups of signals) identified by Dzepina et al. (2007), three were distinctly enriched during HONO events (Fig. 6b); $m/z = 216$, 228, and 240 by 10%, 16%, and 15%, respectively. These signals were also enriched during MRH (Fig. 6a), but not significantly compared to surrounding signals, and are identified as the following PAH compounds: 1,2-benzofluorene, 3,4-benzofluorene, and 1-methylpyrene ($m/z = 216$); benz[α]anthracene, chrysene, and triphenylene ($m/z = 228$); and methylbenzo[*ghi*]fluoranthrene ($m/z = 240$). The distinct X_{event}/X_{MRH} signals suggest that the PAH compounds listed above may be important during events and may contribute to the conversion of HNO_3 to HONO.

PAH compounds having larger m/z were generally enriched during MRH (compared to nMRH) but depleted during HONO events (compared to MRH). Notably, $m/z = 264$, 266, and 278 were enriched during MRH (Fig. 6a) by 74%, 60%, and 78%, respectively, but were depleted during HONO events (Fig. 6b) by 7.3%, 3.6%, and 25%, respectively. These signals likely represent 11H-cyclopenta[*ghi*]perylene, 4H-benzo[*hi*]chrysene, and an unidentified PAH, respectively (Dzepina et al., 2007). Signal at $m/z = 202$ accounted for the highest fraction of the total PAH identified by Dzepina et al. (2007) (the parent-ion for pyrene, fluoranthene, and acephenanthrylene) but was not distinctly enriched during either MRH or events in Houston. Several signals that were significantly enhanced during events could not be attributed to previously identified PAH compounds, notably $m/z = 203$, 219, 235, 261, and 279. These could represent fragments associated with organic compounds of different functionality (including those that are not PAH). While most of the signals at $m/z > 200$ are consistent with PAH identified previously, the emissions contributing to MRH in Houston may differ from those in Mexico City given the proximity of the sampling site to the HSC.

Marr et al. (2006) identified vehicle emissions as the major source for all of the above PAH compounds in Mexico City, based on maximum diurnal concentrations observed during the early morning and good correlation with CO and gas-phase naphthalene. Benzo[*ghi*]perylene is commonly used as a tracer for gasoline vehicles (Zielinska et al., 2004) and was significantly enhanced during the Mexico City morning (Marr et al., 2006). Benzo[*ghi*]-perylene was enriched during MRH in this study by 39% ($m/z = 276$ in Fig. 6a) but only slightly enriched during HONO events (by 3.5%, from Fig. 6b). This may indicate that the organic aerosol composition, and thus HONO formation, was influenced by a more complicated source than simply automobile emissions. Benzo[*ghi*]-perylene could also explain the distinctly high values for X_{MRH}/X_{nMRH} at $m/z = 134$, 136, and 138, which exceeded the X_{MRH}/X_{nMRH} at $m/z = 57$ (Fig. 5a). The mass spectrum for benzo[*ghi*]perylene has strong fragmentation peaks at $m/z = 134$ through 139 (Dzepina et al., 2007) and no other match for these signals was found in Q-AMS spectra published previously (Ulbrich et al., 2008). However, $m/z = 134$, 136, 138 were depleted by 6.6, 4.4, and 3.1%, respectively, in Fig. 5b, supporting the hypothesis that gasoline-powered vehicles are not the sole source that influences HONO events.

The significantly enriched m/z signals during events (Fig. 6b) suggest that PAH compounds may influence heterogeneous HONO formation. The potential for heterogeneous reactions involving PAH compounds is supported by Marr et al. (2006), who suggest that OH is the main oxidant contributing to surface PAH reactions. The enrichment of several PAH parent-ion signals during HONO events (compared to MRH) described here suggests that HNO_3 chemistry also may contribute significantly to PAH processing.

5. Conclusions

Strong temporal correlation was observed between SA and HONO during the early morning, coincident with significant depletion of HNO_3. Molar concentration ratios of HONO to HNO_3 and coincidence with enhanced SA suggest that heterogeneous reactions of HNO_3 are a source of HONO. Mass spectral analysis and strong correlations between SA, organic aerosol, and CO suggest that primarily emitted HOA surface is driving the heterogeneous reactions. HONO concentrations predicted by several heterogeneous mechanisms (using likely conditions) and direct emissions account for only a fraction of those observed. On average, observed HONO was more than a factor of four greater than predicted concentrations using the likely scenario. Predicted HONO concentrations using an upper estimate scenario still result in significant underestimation of HONO concentrations compared to observations. By assuming that all depleted HNO_3 is converted to HONO during nine identified events, the discrepancy between observed and predicted HONO is diminished, as average calculated $HONO_{excess}/HNO_3$ slopes were approximately unity. Deviations from unity likely are due to HNO_3 partitioning into the aerosol phase and due to underestimation of the contribution of NO_2 to HONO formation under certain conditions. Thus, heterogeneous HNO_3 reactions on primary HOA are likely an important source of HONO in urban atmospheres. Observations of HONO formation events prior to sunrise suggest a mechanism that is not photo-dependent. Several PAH compounds were enriched during HONO events, suggesting their importance for HNO_3 conversion. Laboratory work is necessary to investigate HONO formation rates as a function of the chemical composition and oxidation state of HOA. Extrapolation of these results to other urban areas is uncertain, as the influence of the HSC on the observed HONO formation events is not understood. Still, this phenomenon is likely to occur in any urban area where significant HNO_3 is produced or survives through the night and where there is significant emission of HOA.

Acknowledgements

The authors would like to acknowledge funding by Houston Advanced Research Center projects TRAMP (H78) and SHARP (H100) and the Texas Commission on Environmental Quality (Grant No. 582-5-64594-FY07-02). LZ acknowledges financial support during this study from the Office of Oceanic and Atmospheric Research of the National Oceanic and Atmospheric Administration under AIRMAP grant #NA06OAR4600189 to UNH. Use of the AIRMAP Q-AMS is also appreciated. RG acknowledges support of the National Science Foundation through project ATM-0327643. This manuscript has not been reviewed by the funding agencies, and no endorsement should be inferred.

References

Alfarra, M.R., et al., 2004. Characterization of urban and rural organic particulate in the Lower Fraser Valley using two Aerodyne aerosol mass spectrometers. Atmospheric Environment 38 (34), 5745–5758.

Alicke, B., Geyer, A., Hofzumahaus, A., Holland, F., Konrad, S., Patz, H.W., Schafer, J., Stutz, J., Voltz-Thomas, A., Platt, U., 2003. OH formation by HONO photolysis during the Berlioz experiment. Journal of Geophysical Research – Atmospheres 108 (D4), 8247. doi:10.1029/2001JD000579.

Ammann, M., Kalberer, M., Jost, D.T., Tobler, L., Rossler, E., Piguet, D., Gaggeler, H.W., Baltensperger, U., 1998. Heterogeneous production of nitrous acid on soot in polluted air masses. Nature 395 (6698), 157–160.

Ammann, M., Rossler, E., Strekowski, R., George, C., 2005. Nitrogen dioxide multiphase chemistry: uptake kinetics on aqueous solutions containing phenolic compounds. Physical Chemistry Chemical Physics 7 (12), 2513–2518.

Arens, F., Gutzwiller, L., Baltensperger, U., Gäggeler, H.W., Ammann, M., 2001. Heterogeneous reaction of NO_2 on diesel soot particles. Environmental Science & Technology 35 (11), 2191–2199.

Bae, M.S., Schwab, J.J., Zhang, Q., Hogrefe, O., Demerjian, K.L., Weimer, S., Rhoads, K., Orsini, D., Venkatachari, P., Hopke, P.K., 2007. Interference of organic signals in highly time resolved nitrate measurements by low mass resolution aerosol mass spectrometry. Journal of Geophysical Research – Atmospheres 112 (D22). doi:10.1029/2007JD008614.

Canagaratna, M.R., Jayne, J.T., Ghertner, D.A., Herndon, S., Shi, Q., Jimenez, J.L., Silva, P.J., Williams, P., Lanni, T., Drewnick, F., Demerjian, K.L., Kolb, C.E., Worsnop, D.R., 2004. Chase studies of particulate emissions from in-use New York City vehicles. Aerosol Science and Technology 38 (6), 555–573.

Canagaratna, M.R., et al., 2007. Chemical and microphysical characterization of ambient aerosols with the Aerodyne aerosol mass spectrometer. Mass Spectrometry Reviews 26 (2), 185–222.

Clemitshaw, K.C., 2006. Coupling between the tropospheric photochemistry of nitrous acid (HONO) and nitric acid (HNO_3). Environmental Chemistry 3 (1), 31–34.

Dibb, J.E., Scheuer, E., Whitlow, S.I., Vozella, M., Williams, E., Lerner, B.M., 2004. Ship-based nitric acid measurements in the gulf of Maine during New England Air Quality Study 2002. Journal of Geophysical Research – Atmospheres 109 (D20). doi:10.1029/2004JD004843.

Dzepina, K., Arey, J., Marr, L.C., Worsnop, D.R., Salcedo, D., Zhang, Q., Onasch, T.B., Molina, L.T., Molina, M.J., Jimenez, J.L., 2007. Detection of particle-phase polycyclic aromatic hydrocarbons in Mexico City using an aerosol mass spectrometer. International Journal of Mass Spectrometry 263, 152–170.

Finlayson-Pitts, B.J., Wingen, L.M., Sumner, A.L., Syomin, D., Ramazan, K.A., 2003. The heterogeneous hydrolysis of NO_2 in laboratory systems and in outdoor and indoor atmospheres: an integrated mechanism. Physical Chemistry Chemical Physics 5 (2), 223–242.

George, C., Strekowski, R.S., Kleffmann, J., Stemmler, K., Ammann, M., 2005. Photoenhanced uptake of gaseous NO_2 on solid organic compounds: a photochemical source of HONO. Faraday Discussions 130, 195–210.

Gutzwiller, L., Arens, F., Baltensperger, U., Gaggeler, H.W., Ammann, M., 2002. Significance of semivolatile diesel exhaust organics for secondary HONO formation. Environmental Science & Technology 36 (4), 677–682.

Handley, S.R., Clifford, D., Donaldson, D.J., 2007. Photochemical loss of nitric acid on organic films: a possible recycling mechanism for NO_x. Environmental Science & Technology 41 (11), 3898–3903.

Harley, R.A., Hannigan, M.P., Cass, G.R., 1992. Respeciation of organic gas emissions and the detection of excess unburned gasoline in the atmosphere. Environmental Science & Technology 26 (12), 2395–2408.

Harrison, R.M., Peak, J.D., Collins, G.M., 1996. Tropospheric cycle of nitrous acid. Journal of Geophysical Research-Atmospheres 101 (D9), 14429–14439.

Jayne, J.T., Leard, D.C., Zhang, X.F., Davidovits, P., Smith, K.A., Kolb, C.E., Worsnop, D.R., 2000. Development of an aerosol mass spectrometer for size and composition analysis of submicron particles. Aerosol Science and Technology 33 (1–2), 49–70.

Jimenez, J.L., Jayne, J.T., Shi, Q., Kolb, C.E., Worsnop, D.R., Yourshaw, I., Seinfeld, J.H., Flagan, R.C., Zhang, X.F., Smith, K.A., Morris, J.W., Davidovits, P., 2003. Ambient aerosol sampling using the aerodyne aerosol mass spectrometer. Journal of Geophysical Research-Atmospheres 108 (D7). doi:10.1029/2001JD001213.

Kalberer, M., Ammann, M., Arens, F., Gaggeler, H.W., Baltensperger, U., 1999. Heterogeneous formation of nitrous acid (HONO) on soot aerosol particles. Journal of Geophysical Research – Atmospheres 104 (D11), 13825–13832.

Kirchstetter, T.W., Harley, R.A., Littlejohn, D., 1996. Measurement of nitrous acid in motor vehicle exhaust. Environmental Science & Technology 30 (9), 2843–2849.

Kleffmann, J., Becker, K.H., Lackhoff, M., Wiesen, P., 1999. Heterogeneous conversion of NO_2 on carbonaceous surfaces. Physical Chemistry Chemical Physics 1 (24), 5443–5450.

Knipping, E.M., Dabdub, D., 2002. Modeling surface-mediated renoxification of the atmosphere via reaction of gaseous nitric oxide with deposited nitric acid. Atmospheric Environment 36 (36–37), 5741–5748.

Kurtenbach, R., Becker, K.H., Gomes, J.A.G., Kleffmann, J., Lorzer, J.C., Spittler, M., Wiesen, P., Ackermann, R., Geyer, A., Platt, U., 2001. Investigations of emissions and heterogeneous formation of HONO in a road traffic tunnel. Atmospheric Environment 35 (20), 3385–3394.

Lefer, B. and Rappengluck, B., 2009. The TexAQS-II radical and aerosol measurement project (TRAMP). this issue.

Lefer, B., Rappengluck, B., Flynn, J., Haman, C., 2009. Photochemical and meteorological relationships during the TexAQS-II radical and aerosol measurement project. this issue.

Leuchner, M. and Rappengluck, B., 2009. VOC source-receptor relationships in Houston during TexAQS-II. this issue.

Marr, L.C., Dzepina, K., Jimenez, J.L., Reisen, F., Bethel, H.L., Arey, J., Gaffney, J.S., Marley, N.A., Molina, L.T., Molina, M.J., 2006. Sources and transformations of particle-bound polycyclic aromatic hydrocarbons in Mexico City. Atmospheric Chemistry and Physics 6, 1733–1745.

McGaughey, G.R., Desai, N.R., Allen, D.T., Seila, R.L., Lonneman, W.A., Fraser, M.P., Harley, R.A., Pollack, A.K., Ivy, J.M., Price, J.H., 2004. Analysis of motor vehicle emissions in a Houston tunnel during the Texas Air Quality Study 2000. Atmospheric Environment 38 (20), 3363–3372.

Moussiopoulos, N., Papalexiou, S., Lammel, G., Arvanitis, T., 2000. Simulation of nitrous acid formation taking into account heterogeneous pathways: application to the Milan metropolitan area. Environmental Modeling & Software 15 (6–7), 629–637.

Rivera-Figueroa, A.M., Sumner, A.L., Finlayson-Pitts, B.J., 2003. Laboratory studies of potential mechanisms of renoxification of tropospheric nitric acid. Environmental Science & Technology 37 (3), 548–554.

Sage, A.M., Weitkamp, E.A., Robinson, A.L., Donahue, N.M., 2008. Evolving mass spectra of the oxidized component of organic aerosol: results from aerosol mass spectrometer analyses of aged diesel emissions. Atmospheric Chemistry and Physics 8 (5), 1139–1152.

Sarwar, G., Roselle, S.J., Mathur, R., Appel, W., Dennis, R.L., Vogel, B., 2008. A comparison of CMAQ HONO predictions with observations from the Northeast Oxidant and Particle Study. Atmospheric Environment 42 (23), 5760–5770.

Scheuer, E., Talbot, R.W., Dibb, J.E., Seid, G.K., DeBell, L., Lefer, B., 2003. Seasonal distributions of fine aerosol sulfate in the North American Arctic basin during TOPSE. Journal of Geophysical Research – Atmospheres 108 (D4). doi:10.1029/2001JD001364.

Stemmler, K., Ammann, M., Donders, C., Kleffmann, J., George, C., 2006. Photosensitized reduction of nitrogen dioxide on humic acid as a source of nitrous acid. Nature 440 (7081), 195–198.

Stutz, J., Oh, H.-J., Whitlow, S.E., Anderson, C., Dibb, J.E., Flynn, J.H., Rappengluck, B., Lefer, B., 2009. Simultaneous DOAS and Mist-Chamber IC measurements of HONO in Houston, TX. this issue.

Ulbrich, I.M., Canagaratna, M.R., Zhang, Q., Worsnop, D.R., Jimenez, J.L., 2008. Interpretation of organic components from positive matrix factorization of aerosol mass spectrometric data. Atmospheric Chemistry and Physics Discussions 8, 6729–6791.

Vogel, B., Vogel, H., Kleffmann, J., Kurtenbach, R., 2003. Measured and simulated vertical profiles of nitrous acid – part II. Model simulations and indications for a photolytic source. Atmospheric Environment 37 (21), 2957–2966.

Zhang, Q., Alfarra, M.R., Worsnop, D.R., Allan, J.D., Coe, H., Canagaratna, M.R., Jimenez, J.L., 2005a. Deconvolution and quantification of hydrocarbon-like and oxygenated organic aerosols based on aerosol mass spectrometry. Environmental Science & Technology 39 (13), 4938–4952.

Zhang, Q., Worsnop, D.R., Canagaratna, M.R., Jimenez, J.L., 2005b. Hydrocarbon-like and oxygenated organic aerosols in Pittsburgh: insights into sources and processes of organic aerosols. Atmospheric Chemistry and Physics 5, 3289–3311.

Zhou, X.L., Gao, H.L., He, Y., Huang, G., Bertman, S.B., Civerolo, K., Schwab, J., 2003. Nitric acid photolysis on surfaces in low-NO_x environments: significant atmospheric implications. Geophysical Research Letters 30 (23). doi:10.1029/2003GL018620.

Zielinska, B., Sagebiel, J., McDonald, J.D., Whitney, K., Lawson, D.R., 2004. Emission rates and comparative chemical composition from selected in-use diesel and gasoline-fueled vehicles. Journal of Air and Waste Management 54, 1138–1150.